BIOCHEMISTRY
including biophysical chemistry & molecular biology

ARTICLE

pubs.acs.org/biochemistry

The Second Coordination Sphere of FIH Controls Hydroxylation

Evren Saban,[†] Yuan-Han Chen,[‡] John A. Hangasky,[†] Cornelius Y. Taabazuing,[†] Breanne E. Holmes,[†] and Michael J. Knapp*[,†,‡]

[†]Department of Chemistry and [‡]Program in Molecular and Cellular Biology, University of Massachusetts, Amherst, Massachusetts 01003, United States

Supporting Information

ABSTRACT: The factor inhibiting HIF (FIH) is a proximate oxygen sensor for human cells, hydroxylating Asn^{803} within the α-subunit of the hypoxia inducible factor (HIF). FIH is an α-ketoglutatrate (αKG)-dependent, non-heme Fe(II) dioxygenase, in which Fe(II) is coordinated by a (His_2Asp) facial triad, αKG, and H_2O. Hydrogen bonding among the facial triad, the HIF-Asn^{803} side chain, and various second-sphere residues suggests a functional role for the second coordination sphere in tuning the chemistry of the Fe(II) center. Point mutants of FIH were prepared to test the functional role of the αKG-centered (Asn^{205} and Asn^{294}) or HIF-Asn^{803}-centered (Arg^{238} and Gln^{239}) second-sphere residues. The second sphere was tested for local effects on priming Fe(II) to react with O_2, oxidative decarboxylation, and substrate positioning. Steady-sate kinetics were used to test for overall catalytic effects; autohydroxylation rates were used to test for priming and positioning, and electronic spectroscopy was used to assess the primary coordination sphere and the electrophilicity of αKG. Asn^{205} → Ala and Asn^{294} → Ala mutants exhibited diminished rates of steady-state turnover, while minimally affecting autohydroxylation, consistent with impaired oxidative decarboxylation. Blue-shifted metal to ligand charge transfer transitions for (Fe+αKG)FIH indicated that these point mutations destabilized the π^* orbitals of αKG, further supporting a slowed rate of oxidative decarboxylation. The Arg^{238} → Met mutant exhibited steady-state rates too low to measure and diminished product yields, suggesting impaired substrate positioning or priming; the Arg^{238} → Met mutant was capable of O_2 activation for the autohydroxylation reaction. The Gln^{239} → Asn mutant exhibited significantly slowed steady-state kinetics and diminished product yields, suggesting impaired substrate positioning or priming. As HIF binding to the Gln^{239} → Asn mutant stimulated autohydroxylation, it is more likely that this point mutant simply mispositions the HIF-Asn^{803} side chain. This work combines kinetics and spectroscopy to show that these second-sphere hydrogen bonds play roles in promoting oxidative decarboxylation, priming Fe(II) to bind O_2, and positioning HIF-Asn^{803}.

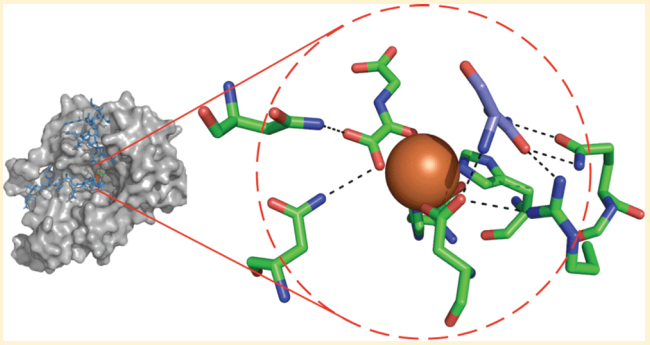

A small number of Fe(II), α-ketoglutarate (αKG)-dependent dioxygenases directly control cellular oxygen sensing in humans.[1−3] These enzymes hydroxylate specific residues within the α-subunit of the hypoxia inducible factor (HIF), thereby affecting the transcriptional level of hundreds of genes.[4] The best characterized of these enzymes is the "factor inhibiting HIF-1" (FIH), which hydroxylates the β-carbon of HIF-Asn^{803};[5] HIF-Asn^{803} lies within the C-terminal transactivation domain (CTAD) of HIFα. Hydroxylating HIF-Asn^{803} turns off HIF-dependent gene expression and is a key step in downregulating angiogenesis. Understanding the chemical basis of how FIH reacts with HIFα and O_2 is crucial to understanding tissue O_2 homeostasis and holds potential for treating disease states such as cancer and stroke.[6−8]

According to the consensus chemical mechanism (Scheme 1), O_2 binds to (Fe^{II}+αKG)FIH only after HIFα binds.[9,10] In this mechanism, the active site Fe(II) of FIH is proposed to change its coordination geometry upon binding HIFα, thereby creating a binding site for O_2. A close correlation between pO_2 and HIF hydroxylation would then result, as the rate would be proportional to pO_2. X-ray crystallography of FIH in various substrate-bound states revealed a structural linkage between HIF binding and O_2 activation through changes in multiple hydrogen bonding interactions.[11−13] Controlling oxygenation chemistry through varied hydrogen bonding to atoms coordinated to the metal has been found in other enzymes and models,[14−16] suggesting that the structural changes in FIH might also be functionally significant.

The chemistry within the FIH active site occurs at the Fe(II) cofactor, making the extended coordination environment of this metal the focus of our investigation. FIH provides a primary coordination sphere of His^{199}, Asp^{201}, and His^{279}, forming a facial triad,[17] with other coordination sites occupied by H_2O or αKG (Figure 1). The secondary coordination sphere is comprised of those residues that form hydrogen bonds to the ligands. Spectroscopic and structural data from FIH and related enzymes suggest

Received: December 22, 2010
Revised: March 24, 2011
Published: April 01, 2011

Scheme 1. Consensus Chemical Mechanism

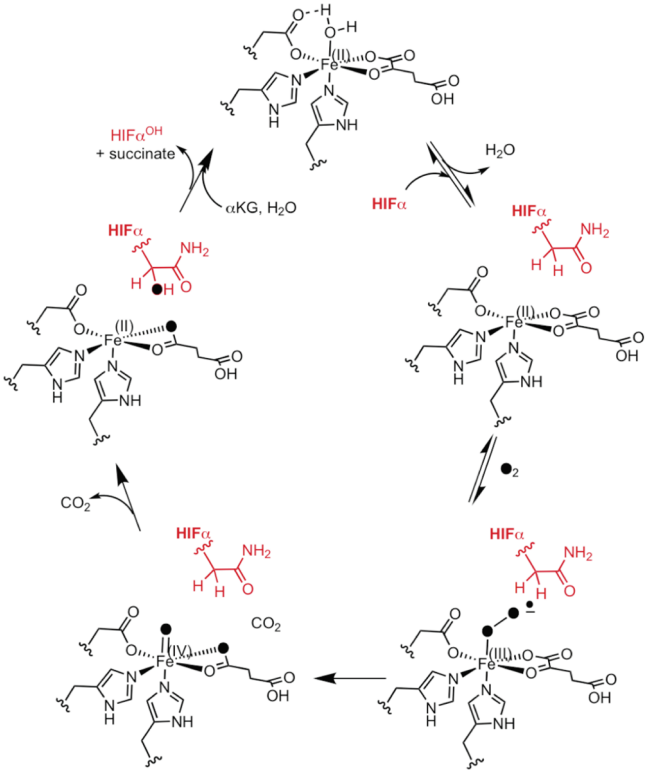

that coordination changes at Fe are crucial to turnover.[9,18,19] On the basis of evidence from related enzymes, these key coordination geometries are proposed to be a six-coordinate (6C) center for (Fe^{II}+αKG)FIH and a five-coordinate (5C) center for (Fe^{II}+αKG+CTAD)FIH.

Hydrogen bonds between surrounding residues, substrates, and iron ligands may comprise a functionally significant second coordination sphere for FIH, both for priming and for oxidative decarboxylation. X-ray crystal structures of FIH imply that the single H_2O ligand is lost from the 6C (Fe^{II}+αKG)FIH upon binding CTAD, which would prime the Fe(II) to react with O_2.[11−13] Concomitant alterations in nearby hydrogen bonds among Arg^{238}, Asp^{201}, and the H_2O ligand suggest that these second-sphere interactions may be necessary for priming. We prepared and characterized the isosteric Arg^{238} → Met mutant to determine how loss of this hydrogen bond linkage affected priming of the Fe(II) to react with O_2.

Decarboxylating α-keto acids generally requires stabilization of negative charge within the transition state.[18−20] Notably, a Lys or Arg is positioned as a hydrogen bond donor to the C1 carboxylate of αKG in most structures of the αKG dioxygenase superfamily.[9] In the case of FIH, Asn^{205} and Asn^{294} appear to fulfill this role by donating hydrogen bonds to the C1 carboxylate. We prepared and characterized the single-point Asn → Ala mutants to test how loss of each hydrogen bond affected O_2 activation in normal turnover as well as autohydroxylation.

Subsequent to O_2 activation, CTAD hydroxylation likely proceeds via a hydrogen transfer and/or rebound steps involving a putative $[FeO]^{2+}$ oxidant observed in related enzymes.[21,22] Precise substrate positioning is necessary to ensure that the putative $[FeO]^{2+}$ oxidant attacks the proper C−H bond. The side chain of the HIFα-Asn^{803} residue is located directly above

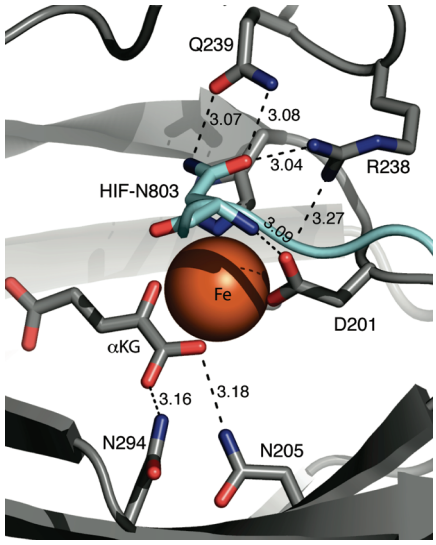

Figure 1. Hydrogen bonding network in the active site of wild-type FIH (Protein Data Bank entry 1H2K). FIH (gray) and CTAD (cyan) are shown as strands; hydrogen bond distances (in angstroms), FIH residues, and HIF-Asn^{803} are denoted.

the open coordination site of the Fe(II) in FIH and forms a hydrogen bond pair with FIH-Gln^{239}. This interaction may be crucial for substrate positioning, such that the $[FeO]^{2+}$ oxidant reacts selectively with the β-carbon of HIF-Asn^{803}. Although Gln^{239} is not strictly a second-sphere residue in FIH, the Gln^{239} → Asn mutant was included in this study as a way to investigate the role of CTAD positioning in catalysis.

Testing the functional role of the second sphere is crucial to understanding the intricate relationship between the overall structure and function of FIH. This work reports the activity, metal binding, and catalytic precision of second-sphere point mutants of FIH. Our results indicate that several second-sphere residues are key to tuning the O_2 reactivity of FIH.

MATERIALS AND METHODS

Protein Expression and Purification. FIH and its mutants were expressed from *Escherichia coli* with an N-terminal His_6 tag and purified as previously described.[23] Following purification via Ni-NTA column chromatography, the His_6 tag was removed by thrombin digestion. Exogenous metal was removed by prolonged incubation with EDTA, and then FIH was further purified by size-exclusion chromatography to yield the FIH dimer.

Differential Scanning Calorimetry (DSC). DSC experiments were performed using a MicroCal VP-DSC microcalorimeter.[24] HEPES buffer (50 mM, pH 7.50) was used, and 50 μM samples were heated in the calorimeter over a 25−75 °C range at a scan rate of 60 °C/h. A buffer scan was subtracted from each data set to correct for baseline drift. Data analysis was performed using Origin Microcal,[25] the results of which are provided in the Supporting Information.

Metal Binding. The experimental protocol was modified from that of Marletta et al.[26] Citrate was used as a chelator to buffer the concentration of free Co(II) ion, $[Co(H_2O)_6]^{2+}$, for which stability constants are reported.[27] Co(II) binding to FIH was monitored by fluorescence quenching in a deoxygenated solution at room temperature. FIH was present in a fluorescence cuvette as a 200 μL solution of 1.00 mM sodium citrate, 20 μM FIH,

Table 1. Kinetic Parameters for WT-FIH and Its Mutants for αKG and the Synthetic Peptide CTAD (39 residues)

	k_{cat} (min^{-1})[a]	$K_{M(\alpha KG)}$ (μM)[b]	$K_{M(CTAD)}$ (μM)[a]	$k_{cat}/K_{M(CTAD)}$ (μM^{-1} min^{-1})[a]
WT-FIH	31 ± 4	22 ± 6	77 ± 22	0.41 ± 0.1
N205A	10.2 ± 0.5	7.5 ± 2	43 ± 8	0.24 ± 0.07
N294A	2.2 ± 0.1	14 ± 2	137 ± 26	0.016 ± 0.004
Q239N	0.123 ± 0.002	24 ± 4	38 ± 2	0.0032 ± 0.0002
R238M[c]	–	–	–	–

[a] Assays in which CTAD was the varied substrate were performed with FIH and mutants (0.5−5 μM), ascorbate (2 mM), DTT (100 μM), catalase (5 units/mL), αKG (500 μM), $FeSO_4$ (25−50 μM), and CTAD (0−600 μM) in 50 mM HEPES (pH 7.50) at 37 °C. CTAD corresponds to a Cys → Ala point mutant of HIF-1α$^{788-826}$. [b] Assays in which αKG was the varied substrate were as described above, with two exceptions: 200 μM CTAD and 3−160 μM αKG. [c] R238M was too slow to assay initial rates.

100 μM α-ketoglutarate, and 50 mM HEPES (pH 7.50). Small volumes of $CoCl_2$ were added from a solution of 1.00 mM $CoCl_2$ and 1.00 mM sodium citrate with 50 mM HEPES (pH 7.50). Following addition of Co(II), the cuvette was gently rocked by hand and the fluorescence measured over several minutes until a steady reading was obtained. Samples were excited at 280 nm, and the fluorescence intensity was measured at 340 nm. Data fitting and results are provided in the Supporting Information.

Electron Paramagnetic Resonance (EPR). X-Band EPR spectra were recorded on a Bruker Elexsys E-500 ESR spectrometer equipped with a Bruker ER 4118CF-O LHe/LN_2 cryostat. EPR samples were prepared by reconstituting enzymes with $CuSO_4$ at a FIH:Cu^{2+} ratio of 1:0.9; the $CuSO_4$ solution was slowly added to the enzyme solution to prevent precipitation. Similarly, (Cu+αKG)FIH was prepared by adding αKG slowly as the final step. Samples totaling 300 μL of 1 mM enzyme, 0.9 mM $CuSO_4$, and 1 mM αKG in 50 mM HEPES (pH 7.50) were frozen in quartz tubes with liquid nitrogen. The spectra were recorded by averaging four scans at a 9.438 GHz frequency, a 20 mW power, a 20 G modulation amplitude, a 100 GHz modulation frequency, and a 327 ms time constant. The microwave power was varied to ensure the samples were not saturated under the reported conditions.

UV−Vis Spectroscopy. Enzyme stocks, $FeSO_4$, and αKG were made anaerobic under an argon flush; 50 mM HEPES (pH 7.50) was also made anaerobic by a repeating cycle of vacuum and nitrogen flush. (Fe^{II}+αKG)FIH spectra were recorded on anaerobic samples containing FIH (250 μM), $FeSO_4$ (230 μM), and αKG (500 μM) in buffer. Apo FIH spectra were recorded for similar samples by omitting αKG and $FeSO_4$ and used as background spectra.

Activity Assays. Initial rate measurements were performed in 50 mM HEPES (pH 7.50) for samples incubated at 37 °C in a 50 μL reaction volume. Reaction buffer included 2.00 mM ascorbate, 100 μM DTT, 5 units/μL catalase, 600 μM αKG, 25 μM $FeSO_4$, and 0−600 μM CTAD peptide was prepared as previously described.[43] The reaction was initiated by addition of the enzyme (0.5−5 μM), and at certain time points, 5 μL aliquots were taken and quenched in 45 μL of 0.1% formic acid. For each reaction, 10 time points were collected and quenched and then analyzed by LC−ESI-MS. Samples were first loaded onto a C8 column for desalting, and CTAD and hydroxylated CTAD ($CTAD^{OH}$) were detected by ESI-MS to determine the mole fraction of peptide that had been converted to product, $\chi_{CTAD\text{-}OH}$. Product concentrations were calculated as $[CTAD^{OH}] = \chi_{(CTAD\text{-}OH)}[CTAD]_0$ and used to determine initial rates, which were then used for Michaelis−Menten fits.

Autohydroxylation. Autohydroxylation was assessed as described previously, with minor changes.[28] FIH (100 μM), $FeSO_4$ (500 μM), and αKG (500 μM) were anaerobically incubated in 50 mM HEPES (pH 7.50) for 20 min. Autohydroxylation was initiated via addition of an equal volume of buffer that had been equilibrated under air, and the reaction was monitored at 583 nm. Competitive autohydroxylation assays included 50 μM CTAD that was preincubated with FIH.

Coupling. A Hamilton PRP-X300 anion exclusion column and UV detection at 210 nm were used to separate and detect the yield of succinate from quenched steady-state reactions of FIH. The concentration of hydroxylated CTAD, $CTAD^{OH}$, was determined as per the activity assays. The coupling ratio (C) was defined as $[succinate]/[CTAD^{OH}]$.

RESULTS

Inspection of the X-ray crystal structure of FIH revealed hydrogen bonding networks surrounding the Fe, which were centered on either αKG or CTAD. Asn^{205} and Asn^{294} residues donate hydrogen bonds to the C1 carboxylate of αKG, suggesting that these second-sphere residues may stabilize charge buildup during decarboxylation. Arg^{238} and Gln^{239} form hydrogen bonds with CTAD, suggesting that these residues may position the HIF-Asn^{803} or may play a role in priming the Fe for oxygenation chemistry (Figure 1). The role of these hydrogen bonds was tested by functional assays and electronic spectroscopy of point mutants.

The effect of the hydrogen bonding network on turnover was investigated by steady-state kinetics (Table 1). Saturating conditions were determined for ascorbate, αKG, and Fe(II), and then initial rates of wild-type FIH (WT-FIH) and its mutants were acquired by varying the CTAD concentration. DTT and catalase were used in the steady-state assays to prevent ferroxidase chemistry by Fe(II) in solution. WT-FIH exhibited a k_{cat} of 31 min^{-1} with a $k_{cat}/K_{M(CTAD)}$ of 0.41 μM^{-1} min^{-1}, similar to previously reported values (Figure 2).[29−31] Each of the mutants had a modest effect on $K_{M(CTAD)}$, as both k_{cat} and k_{cat}/K_M were diminished by a similar factor for each mutant: N205A (3-fold), N294A (15-fold), and Q239N (150-fold) (Figures 2 and 3). R238M exhibited very low activity, which we could detect only through end point assays.

End point assays showed that CTAD-centered mutants were impaired in terms of product yield, relative to WT-FIH and the αKG-centered mutants (Table 2). WT-FIH hydroxylated 94% of CTAD during prolonged incubations; the αKG-centered mutants, N205A and N294A, were nearly as thorough as WT-FIH, converting more than 79% of CTAD to product. In contrast, both CTAD-centered mutants were significantly compromised in their ability to hydroxylate CTAD, as Q239N and R238M converted less than 25% of CTAD to hydroxylated product.

dx.doi.org/10.1021/bi102042t |Biochemistry 2011, 50, 4733–4740

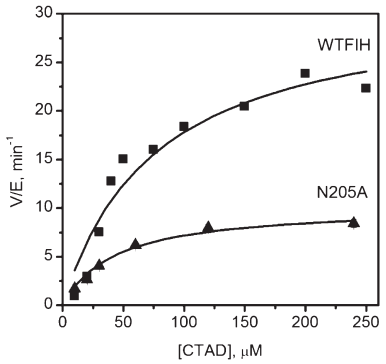

Figure 2. Steady-state kinetics of WT-FIH and N205A. WT-FIH (0.5 μM), N205A (1 μM), ascorbate (2 mM), DTT (100 μM), catalase (5 units/mL), αKG (500 μM), $FeSO_4$ (25 μM), and CTAD (0−250 μM) were in 50 mM HEPES (pH 7.50).

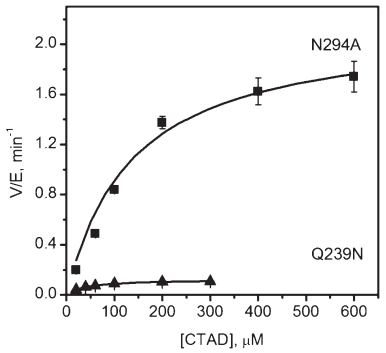

Figure 3. Steady-state kinetics of N294A and Q239N. N294A (5 μM), Q239N (5 μM), ascorbate (2 mM), DTT (100 μM), catalase (5 units/mL), αKG (500 μM), $FeSO_4$ (50 μM), and CTAD (0−600 μM) were in 50 mM HEPES (pH 7.50).

The ratio of succinate production to CTAD hydroxylation was measured, to check for coupling between O_2 activation and hydroxylation (Table 2). As O_2 activation produces succinate but might not lead to hydroxylated CTAD, uncoupling between these two enzymatic steps would lead to elevated coupling ratios (C = [succinate]/[$CTAD^{OH}$]). WT-FIH was tightly coupled,[43] with C equal to unity within experimental uncertainty (C = 0.98 ± 0.03). The Q205A and Q294A point mutants exhibited slightly elevated C values; however, Q239N exhibited a coupling ratio appreciably greater than unity (C = 3.1 ± 0.4).

FIH will slowly activate O_2 in the absence of CTAD, autohydroxylating Trp^{296} to form an Fe(III)-O-Trp^{296} chromophore with a λ_{max} of 583 nm.[23,28] While the rate-limiting step in autohydroxylation is not known, priming of (Fe^{II}+αKG)FIH is a likely requirement to permit O_2 activation. WT-FIH and the point mutants were tested for autohydroxylation rates in the absence of CTAD to determine how the priming of Fe(II) changed upon mutation. The autohydroxylation rates for the point mutants were only moderately altered from that of WT-FIH (Table 3), suggesting that the second coordination sphere had minor effects on steps directly involved in autohydroxylation. It is notable that both αKG-centered mutants exhibited 2-fold increases in the autohydroxylation rates relative to that for WT-FIH.

We felt that a competition assay, in which autohydroxylation was monitored in the presence of CTAD, would be an interesting way to further test the effect of second-sphere mutations on positioning. In the competition assay, $HIF\text{-}Asn^{803}$ and $FIH\text{-}Tr^{296}$ were both present as hydroxylation targets (Table 3). The rate of autohydroxylation for WT-FIH, and those of most of the point mutants, decreased in the presence of CTAD. The lone exception to this was that of the CTAD-centered mutant Q239N, which underwent autohydroxylation 60% faster in the presence of CTAD than in its absence. This increased autohydroxylation rate for Q239N strongly suggested that CTAD binding primed Fe(II) to react with O_2, but that $HIF\text{-}Asn^{803}$ was improperly oriented to receive the oxidant in this point mutant.

The ability of WT-FIH and its mutants to stabilize negative charge on C1 of αKG was analyzed spectroscopically by the energy of the metal to ligand charge transfer (MLCT) transition. UV−vis absorption spectra of the (Fe^{II}+αKG)FIH form of each enzyme were recorded, with the spectrum of the apoenzyme subtracted as a background. Each of the (Fe^{II}+αKG)FIH samples exhibited an MLCT peak near 500 nm (Figure 4). This absorption band has been attributed to three overlapping transitions between populated Fe $T_{2g}(\pi)$ orbitals and empty π^* orbitals delocalized over the C1 carboxylate and C2 keto group of αKG.[18] WT-FIH exhibited an MLCT maximum at 500 nm, similar to that of other αKG hydroxylases such as TauD (530 nm)[32] and CS2 (476 nm).[33] In αKG-centered mutants, this MLCT was blue-shifted (Table 4), with the MLCT peaks for N205A and N294A appearing at 485 and 490 nm, respectively. This blue shift indicated that the αKG π^* orbitals in these point mutants were destabilized from WT-FIH, consistent with the hydrogen bonds donated by Asn^{205} and Asn^{294} pulling electron density away from the keto group of αKG.

Substrate-centered mutations also showed blue-shifted MLCT bands (Table 4). Charge transfer complexes of Q239N and R238M appeared at 495 and 488 nm, respectively. The slight shift in the MLCT energy for Q239N is consistent with the short

Table 2. Coupling and Yield of Hydroxylated CTAD by FIH Variants

	C^a	% $CTAD^{OH}$ [b]
WT-FIH	0.98 ± 0.03	94
N205A	1.08 ± 0.04	90
N294A	1.3 ± 0.1	79
Q239N	3.1 ± 0.4	23
R238M	not determined	5

[a] C = [succinate]/[$CTAD^{OH}$] as determined under steady-state turnover conditions; see the text for details. [b] Qualitative end points: FIH (100 μM) $FeSO_4$ (500 μM), αKG (500 μM), and CTAD (50 μM) in 50 mM HEPES (pH 7.50).

Table 3. Autohydroxylation Rates for FIH Variants[a]

	initial autohydroxylation rates (μM/min)	
	0 μM CTAD	50 μM CTAD
WT-FIH	0.0442 ± 0.0007	0.0265 ± 0.0008
N205A	0.100 ± 0.002	0.078 ± 0.001
N294A	0.0816 ± 0.0008	0.068 ± 0.002
Q239N	0.034 ± 0.001	0.0564 ± 0.0008
R238M	0.0262 ± 0.0008	0.0183 ± 0.0013

[a] In 100 μM FIH, 500 μM $FeSO_4$, 500 μM αKG, 0 or 50 μM CTAD, and 50 mM HEPES (pH 7.50).

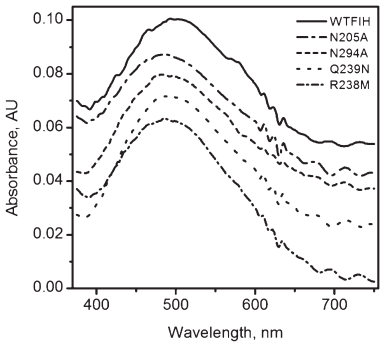

Figure 4. UV−vis spectra of (Fe^{II}+αKG)FIH under anaerobic conditions after subtraction of (Fe^{II})FIH spectra. FIH and mutants (250 μM), $FeSO_4$ (230 μM), and αKG (250 μM) in 50 mM HEPES (pH 7.50).

Table 4. MLCT Transitions in FIH Variants[a]

	λ_{max} (nm)		λ_{max} (nm)
WT-FIH	500	Q239N	495
N205A	485	R238M	488
N294A	490		

[a] In FIH (250 μM), $FeSO_4$ (230 μM), and αKG (250 μM) in 50 mM HEPES (pH 7.50).

distance between residue 239 and αKG, suggesting only minor structural perturbations. The larger shift observed for R238M is similar in magnitude to that observed for N294A and may be tentatively attributed to polarization effects from the loss of the positive charge on residue 238.

Cu(II) was used as a spectroscopic probe for the electronic fine structure in FIH. EPR spectra of both (Cu)FIH and (Cu+αKG)FIH were measured for WT-FIH and each point mutant (Table 5). The spectra of the point mutants were similar to that of WT-FIH, with some heterogeneity evident in the (Cu)FIH samples that diminished significantly in the (Cu+αKG)FIH samples. As FIH provided only three protein-derived ligands, heterogeneity in the (Cu)FIH samples likely arose because of the presence of two or three solvent-derived ligands with variable bond lengths to the Cu(II). The wild-type (Cu)FIH sample exhibited an axial spectrum with apparent g_{eff} and $A_{\|}$ values ($g_{\perp}$ = 2.06; $g_{\|}$ = 2.30; $A_{\|}$ = 146.2 G) appropriate for a "type 2" Cu(II) site with mixed N and O donor ligands (Figure 5).[34] Spectra of the wild-type (Cu+αKG)FIH sample exhibited increased anisotropy in g_{eff} ($g_{\perp}$ = 2.06, and $g_{\|}$ = 2.35) and weakened hyperfine coupling ($A_{\|}$ = 136.4 G) as compared to (Cu)FIH (Figure 6). The small $A_{\|}$ is similar to that reported for other αKG hydroxylases,[35−37] where it was attributed to an O-rich anionic ligand set and distorted planarity.[37] The spectra for the (Cu+αKG)FIH point mutants were nearly identical to those of WT-FIH, showing that the point mutations did not alter the metal coordination geometry in the (Cu+αKG)FIH enzyme form.

Global enzyme stability was not altered by point mutation, as shown by the irreversible melting temperatures [$T_{M(app)}$] determined by DSC (Table S1 of the Supporting Information). The $T_{M(app)}$ of wild-type FIH was 54.5 °C, whereas the $T_{M(app)}$ values for the mutants were, in fact, slightly higher. Substrate-centered mutants R238M and Q239N had $T_{M(app)}$ values slightly higher than that of the wild type (56.2 and 56.7 °C, respectively). The

Table 5. EPR Spectral Parameters[a] **for (Cu)FIH and (Cu+αKG)FIH**

	$g_{\|}$	$g_{\perp}$	$A_{\|}$ (G)
(Cu)FIH	2.30	2.06	146.2
(Cu)N205A	2.31	2.06	131.0
(Cu)N294A	2.31	2.06	134.6
(Cu)Q239N	2.29	2.06	135.0
(Cu)R238M	2.31	2.06	144.8
(Cu+αKG)FIH	2.35	2.06	136.4
(Cu+αKG)N205A	2.35	2.06	136.4
(Cu+αKG)N294A	2.35	2.07	136.4
(Cu+αKG)Q239N	2.35	2.07	136.8
(Cu+αKG)R238M	2.35	2.07	136.1

[a] Parameters observed using Spincount.[44]

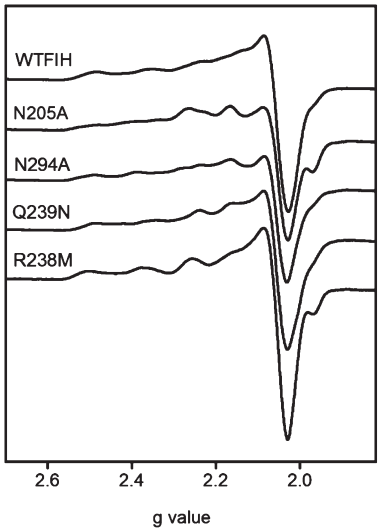

Figure 5. X-Band EPR spectra of (Cu^{II})FIH variants. FIH and point mutants (1 mM) and $CuSO_4$ (0.9 mM) were in 50 mM HEPES (pH 7.50) with a 9.438 GHz frequency, a 20 mW power, a 20 G modulation amplitude, a 100 GHz modulation frequency, and a 327 ms time constant at 77 K.

$T_{M(app)}$ values of αKG-centered mutants N205A and N294A were 58.6 and 58.9 °C, respectively, again indicating that the second-sphere mutations did not alter overall protein stability.

The metal binding of FIH was slightly affected by point mutation, as shown by the Co(II) titrations (Table S2 of the Supporting Information). The equilibrium dissociation constant for (Co^{2+}+αKG)FIH was 1.38(6) × 10^{-7}, indicating a relatively strong affinity for Co^{2+}. Each of the point mutants exhibited a similar dissociation constant, with K_D values ranging from 1.0 to 1.9 × 10^{-7}. This indicated that the primary coordination sphere of the active site was not altered by mutagenesis in the secondary sphere.

DISCUSSION

Hydrogen bonding networks have been shown to be crucial to the function of enzymes reacting with O_2-derived species, such as lipoxygenase and SOD,[15,16] as well as for O_2-activating models.[14]

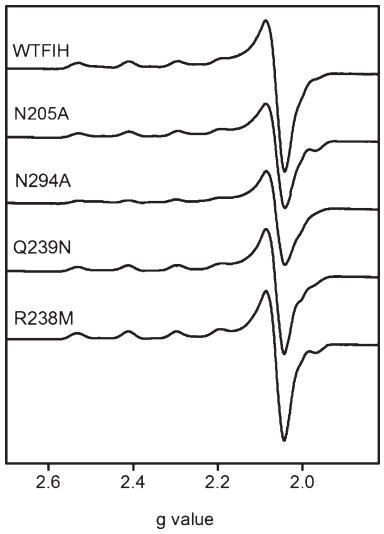

Figure 6. X-Band EPR spectra of $(Cu^{II}+\alpha KG)$FIH variants. FIH and mutants (1 mM), $CuSO_4$ (0.9 mM), and αKG (1 mM) were in 50 mM HEPES (pH 7.50) with a 9.438 GHz frequency, a 20 mW power, a 20 G modulation amplitude, a 100 GHz modulation frequency, and a 327 ms time constant at 77 K.

In the case of FIH, hydrogen bonding was observed among the facial triad ligands of Fe(II), the αKG, and various second-sphere residues, suggesting a functional role in tuning the chemistry of the Fe(II) center. In addition, Gln^{239} forms hydrogen bonds with the CTAD substrate, and its role in substrate positioning has been included. This work combines kinetics and spectroscopy to show that these second-sphere hydrogen bonds play roles in promoting oxidative decarboxylation, priming Fe(II) to bind O_2, and positioning HIF-Asn^{803}.

The steady-state rate constants, k_{cat} and $k_{cat}/K_{M(CTAD)}$, were diminished for each point mutant of FIH (Table 1), indicating a reduction in the rate of one or more steps during turnover. These rate constants can be interpreted within the context of an ordered sequential mechanism, which is the consensus chemical mechanism for αKG hydroxylases.[9,10] A minimal kinetic model (Scheme 2) for FIH in the presence of a saturating level of αKG involves separate microscopic steps for binding CTAD (k_1) and O_2 (k_2), with an irreversible chemical step (k_3) followed by product release (k_4).

The steady-state rate constants are composites of the microscopic steps described above. All steps after substrate binding contribute to k_{cat}, while $k_{cat}/K_{M(CTAD)}$ is a function of all steps up through the first irreversible step. The reduced values of both k_{cat} and $k_{cat}/K_{M(CTAD)}$ for each point mutant suggest that the second coordination sphere plays a significant role in determining k_3, the common microscopic step. This first irreversible step may be oxidative decarboxylation of αKG to form the $[FeO]^{2+}$ intermediate, as seen for TauD,[38,39] or another step forming an Fe(II) center, as implied for PHD.[40] In the absence of additional mechanistic probes such as kinetic isotope effects, we turned to the use of electronic spectroscopy and inactivation kinetics to test the effect of the second-sphere residues.

Point mutations of second-sphere residues were nonperturbing with respect to the protein structure and primary coordination of the metal center in mutated FIH, as shown by the thermodynamic stability and electronic spectroscopy of each mutant. EPR spectra of the point mutants showed that the metal center in $(Cu+\alpha KG)$FIH retained a ground-state electronic

Scheme 2.

$$E \underset{}{\overset{k_1}{\rightleftharpoons}} ES \overset{k_2}{\rightleftharpoons} ES(O_2) \xrightarrow{k_3} \xrightarrow{k_4} E + P$$

environment virtually identical to that of WT-FIH (Figure 6). The MLCT transitions for $(Fe^{II}+\alpha KG)$FIH variants revealed that αKG was a bidentate ligand to Fe(II), while also providing a view of the changing Lewis acidity of the C2 position of αKG (Figure 4). As nucleophilic attack of superoxide at C2 is thought to be a key step in O_2 activation by αKG-dependent oxygenases,[41] the Lewis acidity of the keto group is essential for oxidative decarboxylation. The blue shifts in the MLCT energies for point mutants indicated that the αKG π^* orbitals were destabilized in the N294A and N205A mutants, suggesting that the hydrogen bonds found in WT-FIH serve to pull electron density away from the C2 position of αKG.

Oxidative decarboxylation is promoted by stabilizing negative charge buildup in the transition state, as shown for enzymes[20] and model complexes.[41] Structural analysis and the MLCT shifts in FIH indicate that both Asn^{205} and Asn^{294} pull electron density away from αKG, although the Fe(II) likely plays the predominant role in activating αKG for decarboxylation. Asn^{294} plays a more significant role than Asn^{205} in stabilizing charge, as shown by the relative values of k_{cat}: WT-FIH > N205A > N294A (Table 1). This may be due to Asn^{294} being the sole residue pulling electron density away from the distal O of the C1 carboxylate of αKG, while both Asn^{205} and Fe(II) pull electron density from the proximal O of the C1 carboxylate (Figure 1).

The significant decrease in the steady-state rate constants for CTAD-centered mutants may arise from changes in Fe(II) priming or CTAD positioning. The consensus chemical mechanism suggests that mutations affecting priming should principally reduce $k_{cat}/K_{M(CTAD)}$, as steps up through O_2 activation determine this rate constant. Conversely, mutations affecting positioning should reduce k_{cat}, as steps following O_2 binding determine this rate constant. Although the structure of FIH with CTAD bound suggests that there may be hydrogen bonds with specific roles, such as those between Gln^{239} and HIF-Asn^{803} (positioning), and between Arg^{238} and Asp^{201} (priming), the kinetics data are less clear as each point mutation reduced k_{cat} as well as $k_{cat}/K_{M(CTAD)}$ when compared to those of WT-FIH. This may arise from an effect on a chemical step common to both rate constants, such as O_2 activation, or from the extended hydrogen bond network linking Asp^{201} to HIF-Asn^{803} through Arg^{238} and Gln^{239} (Figure 1). It appears that positioning the side chain of HIF-Asn^{803} is integral to the priming of Fe(II) and may even be a design feature to ensure tight coupling between O_2 activation and substrate hydroxylation.

While priming could not be separated from substrate positioning by steady-state kinetics, the two roles could be distinguished by the coupling ratio and by analysis of hydroxylation products, as shown for TauD.[42] A functional view of priming is the abilty of FIH to activate O_2 only once CTAD binds, leading to close coupling between the production of succinate and $CTAD^{OH}$. In the case of WT-FIH, breakdown in priming leads solely to autohydroxylation as FIH does not release reactive oxygen species.[23,28,43] This was supported by our observation of a coupling value of unity ($C = 0.98 \pm 0.03$) for WT-FIH, and a near-unity coupling ratio for N205A and N294A.

Positioning HIF-Asn^{803} in the proper registry within the active site is crucial to ensuring that the $[FeO]^{2+}$ oxidant attacks the

correct residue and forms the $CTAD^{OH}$ product. The Q239N mutant exhibited notable effects on the coupling ratio, indicating that Gln^{239} was crucial for local positioning (Table 2). Q239N was the only mutant in which the coupling ratio differed significantly from unity (3.1 ± 0.4), and the only mutant that autohydroxylated faster in the presence of CTAD. These observations indicate that, while Q239N was able to activate O_2, the HIF-Asn^{803} side chain was improperly positioned to form the normal product.

FIH serves a crucial role in sensing hypoxia within human cells. As an O_2-sensing enzyme, it must maintain tight coupling between O_2 activation and substrate hydroxylation, which it achieves by hydrogen bonding between ligands to the Fe and the second coordination sphere. These second-sphere hydrogen bonds play roles in promoting O_2 activation as well as maintaining the structural registry between CTAD and Fe. Hydrogen bonds from Asn^{205} and Asn^{294} pulled electron density away from αKG, as shown by the LMCT transitions; removal of either hydrogen bond from the Asn → Ala point mutants slighly accelerated autohydroxylation but made normal turnover much slower in the case of the Asn^{294} → Ala mutant. It is likely that autohydroxylation rates reflect the intrinsic reactivity of αKG, whereas the rate of normal turnover is more dependent on the precise positioning of CTAD. For this reason, the rate constants for normal turnover are greatly reduced in Gln^{239} → Asn and Arg^{238} → Met mutants, both CTAD-centered mutants. By virtue of their respective locations relative to Asp^{201} and HIF-Asn^{803}, it is likely that Arg^{238} is necessary for priming of the Fe(II) in response to CTAD binding, whereas Gln^{239} is more involved in positioning HIF-Asn^{803}. The second-sphere interactions play a significant role in the O_2 sensing function of FIH by tuning the chemistry at the Fe(II) center.

■ ASSOCIATED CONTENT

Ⓢ Supporting Information. Tabulated results for thermal melting (DSC) and Co(II) binding titrations for FIH variants. This material is available free of charge via the Internet at http://pubs.acs.org.

■ AUTHOR INFORMATION

Corresponding Author

*Phone: (413) 545-4001. Fax: (413) 545-4490. E-mail: mknapp@chem.umass.edu.

Funding Sources

Supported by National Institutes of Health Grant R01-GM077413.

■ ACKNOWLEDGMENT

We thank the National Science Foundation for the support of the EPR facility (CHE-0443180 NSF-CRIF) and Prof. Stephen Eyles for technical assistance.

■ ABBREVIATIONS

αKG, α-ketoglutarate; CTAD, C-terminal transactivation domain of HIFα; DSC, differential scanning calorimetry; EPR, electron paramagnetic resonance; FIH, factor inhibiting HIF-1; HIF, hypoxia inducible factor; LC−ESI-MS, liquid chromatography−electrospray ionization mass spectrometry; MLCT, metal to ligand charge transfer; NTA, nitrilotriacetate; SOD, superoxide dismutase.

■ REFERENCES

(1) Bruick, R. K., and McKnight, S. L. (2001)A conserved family of prolyl-4-hydroxylases that modify HIF. *Science 294*, 1337–1340.

(2) Ozer, A., and Bruick, R. K. (2007)Non-heme dioxygenases: Cellular sensors and regulators jelly rolled into one? *Nat. Chem. Biol. 3*, 144–153.

(3) Semenza, G. L. (2004)Hydroxylation of HIF-1: Oxygen sensing at the molecular level. *Physiology 19*, 176–182.

(4) Mole, D. R., Blancher, C., Copley, R. R., Pollard, P. J., Gleadle, J. M., Ragoussis, J., and Ratcliffe, P. J. (2009)Genome-wide Association of Hypoxia-inducible Factor (HIF)-1α and HIF-2α DNA Binding with Expression Profiling of Hypoxia-inducible Transcripts. *J. Biol. Chem. 284*, 16767–16775.

(5) McNeill, L. A., Hewitson, K. S., Claridge, T. D., Seibel, J. F., Horsfall, L. E., and Schofield, C. J. (2002)Hypoxia-inducible factor asparaginyl hydroxylase (FIH-1) catalyses hydroxylation at the β-carbon of asparagine-803. *Biochem. J. 367*, 571–575.

(6) Hanauske-Abel, H. M., and Gunzler, V. (1982)A stereochemical concept for the catalytic mechanism of prolylhydroxylase: Applicability to classification and design of inhibitors. *J. Theor. Biol. 94*, 421–455.

(7) Hewitson, K. S., and Schofield, C. J. (2004)The HIF pathway as a therapeutic target. *Drug Discovery Today 9*, 704–711.

(8) Nagel, S., Talbot, N. P., Mecinovic, J., Smith, T. G., Buchan, A. M., and Schofield, C. J. (2010)Therapeutic Manipulation of the HIF Hydroxylases. *Antioxid. Redox Signaling 12*, 481–501.

(9) Hausinger, R. P. (2004)FeII/α-ketoglutarate-dependent hydroxylases and related enzymes. *Crit. Rev. Biochem. Mol. Biol. 39*, 21–68.

(10) Solomon, E. I., Brunold, T. C., Davis, M. I., Kemsley, J. N., Lee, S. K., Lehnert, N., Neese, F., Skulan, A. J., Yang, Y. S., and Zhou, J. (2000) Geometric and electronic structure/function correlations in non-heme iron enzymes. *Chem. Rev. 100*, 235–350.

(11) Dann, C. E., Bruick, R. K., and Deisenhofer, J. (2002)Structure of factor-inhibiting hypoxia-inducible factor 1: An asparaginyl hydroxylase involved in the hypoxic response pathway. *Proc. Natl. Acad. Sci. U.S.A. 99*, 15351–15356.

(12) Elkins, J. M., Hewitson, K. S., McNeill, L. A., Seibel, J. F., Schlemminger, I., Pugh, C. W., Ratcliffe, P. J., and Schofield, C. J. (2003) Structure of factor-inhibiting hypoxia-inducible factor (HIF) reveals mechanism of oxidative modification of HIF-1α. *J. Biol. Chem. 278*, 1802–1806.

(13) Lee, C., Kim, S. J., Jeong, D. G., Lee, S. M., and Ryu, S. E. (2003) Structure of human FIH-1 reveals a unique active site pocket and interaction sites for HIF-1 and von Hippel-Lindau. *J. Biol. Chem. 278*, 7558–7563.

(14) Shook, R. L., and Borovik, A. S. (2008)The effects of hydrogen bonds on metal-mediated O_2 activation and related processes. *Chem. Commun.*, 6095–6107.

(15) Tomchick, D. R., Phan, P., Cymborowski, M., Minor, W., and Holman, T. R. (2001)Structural and functional characterization of second-coordination sphere mutants of soybean lipoxpgenase-1. *Biochemistry 40*, 7509–7517.

(16) Miller, A. F. (2008)Redox tuning over almost 1 V in a structurally conserved active site: Lessons from Fe-containing superoxide dismutase. *Acc. Chem. Res. 41*, 501–510.

(17) Hegg, E. L., and Que, L. (1997)The 2-His-1-carboxylate facial triad: An emerging structural motif in mononuclear non-heme iron(II) enzymes. *Eur. J. Biochem. 250*, 625–629.

(18) Pavel, E. G., Zhou, J., Busby, R. W., Gunsior, M., Townsend, C. A., and Solomon, E. I. (1998)Circular dichroism and magnetic circular dichroism spectroscopic studies of the non-heme ferrous active site in clavaminate synthase and its interaction with α-ketoglutarate cosubstrate. *J. Am. Chem. Soc. 120*, 743–753.

(19) Zhou, J., Kelly, W. L., Bachmann, B. O., Gunsior, M., Townsend, C. A., and Solomon, E. I. (2001)Spectroscopic studies of substrate interactions with clavaminate synthase 2, a multifunctional α-KG-dependent non-heme iron enzyme: Correlation with mechanisms and reactivities. *J. Am. Chem. Soc. 123*, 7388–7398.

(20) Walsh, C. T. (1979) *Enzymatic Reaction Mechanisms*, W. H. Freeman & Co., San Francisco.

(21) Price, J. C., Barr, E. W., Tirupati, B., Bollinger, J. M., Jr., and Krebs, C. (2003)The first direct characterization of a high-valent iron intermediate in the reaction of an α-ketoglutarate-dependent dioxygenase: A high-spin FeIV complex in taurine/α-ketoglutarate dioxygenase (TauD) from *Escherichia coli*. *Biochemistry 42*, 7497–7508.

(22) Proshlyakov, D. A., Henshaw, T. F., Monterosso, G. R., Ryle, M. J., and Hausinger, R. P. (2004)Direct detection of oxygen intermediates in the non-heme Fe enzyme taurine/α-ketoglutarate dioxygenase. *J. Am. Chem. Soc. 126*, 1022–1023.

(23) Chen, Y. H., Comeaux, L. M., Herbst, R. W., Saban, E., Kennedy, D. C., Maroney, M. J., and Knapp, M. J. (2008)Coordination changes and auto-hydroxylation of FIH-1: Uncoupled O_2-activation in a human hypoxia sensor. *J. Inorg. Biochem. 102*, 2120–2129.

(24) Plotnikov, V. V., Brandts, J. M., Lin, L. N., and Brandts, J. F. (1997)A new ultrasensitive scanning calorimeter. *Anal. Biochem. 250*, 237–244.

(25) *Origin* (2010) OriginLab Corp., Northampton, MA.

(26) Mills, S. A., and Marletta, M. A. (2005)Metal binding characteristics and role of iron oxidation in the ferric uptake regulator from *Escherichia coli*. *Biochemistry 44*, 13553–13559.

(27) Martell, A. E., and Smith, R. M. (1974) *Critical Stability Constants*, Plenum Press, New York.

(28) Chen, Y. H., Comeaux, L. M., Eyles, S. J., and Knapp, M. J. (2008)Auto-hydroxylation of FIH-1: An Fe(II), α-ketoglutarate-dependent human hypoxia sensor. *Chem. Commun.*, 4768–4770.

(29) Ehrismann, D., Flashman, E., Genn, D. N., Mathioudakis, N., Hewitson, K. S., Ratcliffe, P. J., and Schofield, C. J. (2007)Studies on the activity of the hypoxia-inducible-factor hydroxylases using an oxygen consumption assay. *Biochem. J. 401*, 227–234.

(30) Koivunen, P., Hirsila, M., Gunzler, V., Kivirikko, K. I., and Myllyharju, J. (2004)Catalytic properties of the asparaginyl hydroxylase (FIH) in the oxygen sensing pathway are distinct from those of its prolyl 4-hydroxylases. *J. Biol. Chem. 279*, 9899–9904.

(31) Linke, S., Stojkoski, C., Kewley, R. J., Booker, G. W., Whitelaw, M. L., and Peet, D. J. (2004)Substrate requirements of the oxygen-sensing asparaginyl hydroxylase factor-inhibiting hypoxia-inducible factor. *J. Biol. Chem. 279*, 14391–14397.

(32) Ryle, M. J., Padmakumar, R., and Hausinger, R. P. (1999) Stopped-Flow Kinetic Analysis of *Escherichia coli* Taurine/α-Ketoglutarate Dioxygenase: Interactions with α-Ketoglutarate, Taurine, and Oxygen. *Biochemistry 38*, 15278–15286.

(33) Zhou, J., Gunsior, M., Bachmann, B. O., Townsend, C. A., and Solomon, E. I. (1998)Substrate Binding to the α-Ketoglutarate-Dependent Non-Heme Iron Enzyme Clavaminate Synthase 2: Coupling Mechanism of Oxidative Decarboxylation and Hydroxylation. *J. Am. Chem. Soc. 120*, 13539–13540.

(34) Peisach, J., and Blumberg, W. E. (1974)Structural Implications Derived from Analysis of Electron-Paramagnetic Resonance-Spectra of Natural and Artificial Copper Proteins. *Arch. Biochem. Biophys. 165*, 691–708.

(35) Bleijlevens, B., Shivarattan, T., Sedgwick, B., Rigby, S. E. J., and Matthews, S. J. (2007)Replacement of non-heme Fe(II) with Cu(II) in the α-ketoglutarate dependent DNA repair enzyme AlkB: Spectroscopic characterization of the active site. *J. Inorg. Biochem. 101*, 1043–1048.

(36) Hegg, E. L., Whiting, A. K., Saari, R. E., McCracken, J., Hausinger, R. P., and Que, L. (1999)Herbicide-degrading α-keto acid-dependent enzyme TfdA: Metal coordination environment and mechanistic insights. *Biochemistry 38*, 16714–16726.

(37) Whiting, A. K., Que, L., Saari, R. E., Hausinger, R. P., Fredrick, M. A., and McCracken, J. (1997)Metal coordination environment of a Cu(II)-substituted α-keto acid-dependent dioxygenase that degrades the herbicide 2,4-D. *J. Am. Chem. Soc. 119*, 3413–3414.

(38) Grzyska, P. K., Ryle, M. J., Monterosso, G. R., Liu, J., Ballou, D. P., and Hausinger, R. P. (2005)Steady-state and transient kinetic analyses of taurine/α-ketoglutarate dioxygenase: Effects of oxygen concentration, alternative sulfonates, and active-site variants on the fe(IV)-oxo intermediate. *Biochemistry 44*, 3845–3855.

(39) Price, J. C., Barr, E. W., Glass, T. E., Krebs, C., and Bollinger, J. M., Jr. (2003)Evidence for hydrogen abstraction from C1 of taurine by the high-spin Fe(IV) intermediate detected during oxygen activation by taurine:α-ketoglutarate dioxygenase (TauD). *J. Am. Chem. Soc. 125*, 13008–13009.

(40) Flashman, E., Hoffart, L. M., Hamed, R. B., Bollinger, J. M., Krebs, C., and Schofield, C. J. (2010)Evidence for the slow reaction of hypoxia-inducible factor prolyl hydroxylase 2 with oxygen. *FEBS J. 277*, 4089–4099.

(41) Mehn, M. P., Fujisawa, K., Hegg, E. L., and Que, L. (2003) Oxygen activation by nonheme iron(II) complexes: α-Keto carboxylate versus carboxylate. *J. Am. Chem. Soc. 125*, 7828–7842.

(42) McCusker, K. P., and Klinman, J. P. (2010)An Active-Site Phenylalanine Directs Substrate Binding and C-H Cleavage in the α-Ketoglutarate-Dependent Dioxygenase TauD. *J. Am. Chem. Soc. 132*, 5114–5120.

(43) Saban, E., Flagg, S. C., and Knapp, M. J. (2011) *J. Inorg. Biochem. 105*, 630–636.

(44) Hendrich, M. P. (2010) *Spincount*, Carnegie Mellon University, Pittsburgh, PA.